

# Deformation of the Upper Surface of an Airfoil by Macro Fiber Composite Actuators

Marco Debiasi<sup>1</sup> and Yann Bouremel<sup>2</sup>

*Temasek Laboratories, National University of Singapore, Singapore, 117411*

Hock Hee Khoo<sup>3</sup> and Siao Chung Luo<sup>4</sup>

*Department of Mechanical Engineering, National University of Singapore, Singapore, 117576*

**In this follow-on study, macro fiber composite actuators are used to change the shape of the upper surface of an airfoil model with geometry close to that of the NACA 4415 type. In the design discussed, these thin and light piezoelectric actuators are bonded to the inside and become an integral part of the skin of the upper surface of the airfoil. The model used in this study incorporates some structural changes that allow a smoother shaping of the surface closer to the leading edge of the airfoil. Still-air and wind-tunnel measurements in different flow regimes are performed to assess the characteristics of the deformation of the upper surface. The results obtained can be used to design a wing with morphing upper surface for improved aerodynamics, for maneuvering without ailerons, and/or for active control of the flow over the wing.**

## Nomenclature

$c$	=	model chord
$C_D$	=	drag coefficient
$C_L$	=	lift coefficient
$C_M$	=	pitching-moment coefficient about $c/4$
$D$	=	drag force
$L$	=	lift force
$l$	=	local coordinate tangent to the airfoil surface
$n$	=	local coordinate normal to the airfoil surface
$Re_c$	=	Reynolds number based on the chord
$s$	=	model span (from wall to wall of the wind tunnel)
$U$	=	flow velocity
$x$	=	streamwise coordinate of the wind tunnel
$y$	=	spanwise coordinate of the wind tunnel
$z$	=	vertical coordinate of the wind tunnel

### Greek letters

$\alpha$	=	angle of attack of the airfoil
$\xi$	=	axial (chordwise) coordinate of the airfoil
$\zeta$	=	normal coordinate of the airfoil

### Subscripts

$cp$	=	center of pressure
$\infty$	=	freestream conditions

<sup>1</sup> Senior Research Scientist, Temasek Laboratories, National University of Singapore, Singapore, Member AIAA.

<sup>2</sup> Research Scientist, Temasek Laboratories, National University of Singapore, Singapore, Member AIAA.

<sup>3</sup> Graduate Student, Department of Mechanical Engineering, National University of Singapore, Singapore.

<sup>4</sup> Associate Professor, Department of Mechanical Engineering, National University of Singapore, Singapore.

## I. Introduction

THE ability to change the shape of a wing allows adapting it to different flight conditions. Birds, bats, and insects have developed through evolution wings capable of dramatic and continuous morphing not only for generating the lift required to stay aloft, but also to propel themselves in the air and to perform controlled maneuvers. To a smaller extent the wings of aircraft can also achieve discrete changes of their shape by using ailerons, flaps, and slats or by modifying their sweep, dihedral, or incidence angle. Thus much research is devoted to understand and optimize extensive types of wing morphing for improving the aircraft performance.<sup>1-6</sup> However, extensive wing morphing poses significant design challenges and requires complex mechanical structures and actuators. By contrast limited but continuous morphing of a wing can often be sufficient for the needs of flight (as shown by the minimal movements of the wings of various birds in some flight conditions). The selective displacement of an airfoil upper surface by less than 0.5 % of its chord is sufficient to introduce changes of the pressure distribution useful for tailoring the lift and drag coefficients at high-subsonic speed.<sup>7</sup> This can be used to optimize the performance of an airfoil around a design point, for instance at cruise conditions. Asymmetric changes in the left and right wing can also be used to maneuver an aircraft without using ailerons. Larger displacements would be required at lower speed, but still within a few percent of a wing chord. Furthermore, limited shape changes appear more feasible for actuation at high frequencies.<sup>8</sup> This can be exploited to actively control some undesirable phenomena of the wings like flow separation<sup>9-11</sup> and aeroelastic oscillations.<sup>12-14</sup>

A major difficulty in implementing wing morphing is represented by the size, weight, complexity, and power<sup>15</sup> demanded by the appropriate actuators (hydraulic, pneumatic, electric motors, or even some smart materials like shape-memory alloys). From a system-integration point of view, the performance increase offered by the morphing must outweigh its associated penalties. In this respect, limited morphing is also appealing as it may offer useful aerodynamic advantages with small, light, simple, and power-saving actuators.

The macro fiber composite (MFC) actuators, originally developed at NASA, belong to this category and seem promising for implementing different types of wing morphing, especially if limited shape changes are required. These thin, light, and flexible piezoelectric actuators, Fig. 1, consist of rectangular piezo-ceramic rods sandwiched between layers of adhesive and electroded polyimide film which contains interdigitated electrodes that transfer the applied voltage directly to the rods. When embedded in a surface or attached to flexible structures, the MFCs provide distributed deflection and vibration control. They can also be used as sensors to measure the structural strain under applied loads.

Some studies have explored the use of such actuators to change or control the shape of aerodynamic bodies. Munday et al. used THUNDER actuators (a predecessor of the MFC type, also developed at NASA) to increase the lift of an airfoil.<sup>9-11</sup> Their morphing airfoil model is based on a prototype made by Pinkerton and Moses.<sup>16</sup> Static and dynamic morphing tests were conducted at angles of attack from 0° to 9° at low Reynolds numbers of  $2.5 \cdot 10^4$  and  $5 \cdot 10^4$ . Static morphing shows modest aerodynamic benefits with best increase of the  $L/D$  ratio of about 2%. However, dynamic morphing significantly reduces the size of flow separation therefore greatly increasing the  $L/D$  ratio. Bilgen et al. investigated the use of MFCs to change the wing camber for roll and pitch control of a remotely piloted micro-air-vehicle (MAV).<sup>17</sup> The MAV was flown successfully and demonstrated sufficient roll control in flight as well as in the wind tunnel. It survived numerous crashes proving the durability of MFCs. Successively, Bilgen et al. investigated in detail the use of MFCs to change the camber of a symmetric airfoil.<sup>18</sup> The progress of this research led to the fabrication and flight demonstration of a small aircraft with solid-state control surfaces.<sup>19</sup> More recently, Bilgen et al. developed a novel design for a variable-camber airfoil employing a continuous inextensible surface with bonded MFC actuators which can achieve significant change in aerodynamic response.<sup>20</sup> Moses et al. studied MFC actuators as a mean for reducing buffeting loads on a twin-tail fighter aircraft flying at high angles of attack.<sup>21</sup> Wind-tunnel tests with open and closed-loop buffet alleviation have shown buffeting reductions of over 80%.

The main scope of this follow-on project is to explore the use of MFC actuators integrated to the upper skin of a wing for changing the shape of its upper surface to the degree required for tailoring the wing's performance. To some extent this work parallels those of Munday et al. However the actuators used in this case are more advanced. Also, their integration in the wing structure is simpler and requires negligible space and minimal weight which are very desirable characteristics for practical implementation in aircraft.

## II. Experimental Setup

An airfoil model has been fabricated for testing the shape changes of its upper surface by MFC actuators, Figs. 2 and 3. The model chord  $c$  is 150 mm and its span  $s$  is 158 mm. This model incorporates some structural and fabrication improvements compared to the model used in a previous study.<sup>22</sup> A 0.25 mm-thick carbon-fiber sheet, a material suitable for fabricating the skin of small aircraft, has been used for the upper skin. This is not directly bonded to the model structure but it is connected to it through a 0.25 mm brass shim which wraps around the leading edge, Figs. 2 and 3a). This arrangement allows more flexibility and the bending of the skin is closer to the leading edge compared to the previous model. A vacuum-bag was used to bond the MFC patches (Smart Material M-8557-P1) to the inner side of the skin, Fig. 3b). This bonding process avoids inducing micro-cracks in the MFC's piezo-ceramic rods thus enabling them to safely withstand sinusoidal actuation at different frequencies and amplitudes. The geometry of the airfoil without MFC actuation is slightly flatter than that of a NACA 4415 airfoil. The skin deflects inward when a positive voltage is applied to the MFCs, whereas it deflects outward when a negative voltage is applied, Fig. 2. The displacement causes the skin to have a small variation in the longitudinal direction which is accommodated by allowing it to slide in a thin pocket at the trailing edge.

The MFC actuators are driven by a Smart Material HVA 1500/50-2 high-voltage amplifier which is designed to power a number of different piezo-actuators. This unit has a voltage gain of 200 V / V and a signal bandwidth from DC to 10 kHz depending on the load capacitance. It accepts input voltages in the range from -2.5 V to 7.5 V which are amplified to values of -500 V to 1500 V, the voltage range of the MFC actuators.

The aerodynamic characteristics of the model have been tested in the small, open-loop, subsonic wind tunnel of the NUS Temasek Laboratories, Fig. 4. The range of the wind-tunnel freestream velocity  $U_\infty$  is 2 to 35 m/s. Square test sections with width and height of 160 mm and different lengths can be connected to the exit of the wind-tunnel nozzle which has a 9.8:1 contraction ratio. The turbulence intensity level of the wind-tunnel freestream is less than 0.25%. The leading edge of the model was located 200 mm downstream of the nozzle. In this location the boundary-layer thickness of the empty test section is less than 3 mm for values of  $U_\infty$  between 10 to 20 m/s. The nominal velocity of the flow upstream of the model was obtained by measuring its total pressure with a pitot intake upstream of the nozzle (and downstream of the settling chamber meshes) and its static pressure with a tap located in the wall of the test section 120 mm downstream of the nozzle. The total and static pressure ports were connected to an Exttech HD350 digital anemometer. This arrangement permitted controlling and maintaining the flow velocity within  $\pm 0.1$  m/s.

The displacement of the upper skin with actuation of the MFCs was measured with a Micro-Epsilon optoNCDT 1710-50 laser displacement sensor. This unit has a measuring range between 550 and 600 mm with a resolution of 5  $\mu\text{m}$  and an accuracy of 50  $\mu\text{m}$ . The measuring range allows it to be placed outside the wind-tunnel thus enabling measurements of the skin displacement in the flow. These were acquired at 312.5 Hz simultaneously to the corresponding values of the actuation voltage.

The model was mounted on a turntable incorporating a balance. The turntable allows precise positioning (within  $\pm 0.2^\circ$ ) of the angle of attack  $\alpha$  of the model. The balance consists of a Gamma ATI SI-65-5 piezoelectric gauge. This unit can measure the forces and the moments along three perpendicular axes. We used two axes aligned with the streamwise and the vertical directions of the wind tunnel to measure the drag and the lift forces generated by the model. The third axis, coinciding with the axis of rotation of the turntable and aligned in the spanwise direction, passed through the airfoil mid-chord point ( $c/2$ ) and was used to measure the pitching moment. The balance was factory calibrated and the corresponding conversion factors stored in the acquisition unit used with it such that the values of the forces and moments obtained are already corrected. The range (and accuracy) of the measured forces and moment are 65 ( $\pm 1/80$ ) N and 5 ( $\pm 8 \cdot 10^{-4}$ ) Nm, respectively. For each measurement, 2048 samples of the values of the forces and moment were acquired at 2 kHz and low-pass filtered at 10 Hz before averaging in order to remove the effect of small vibrations induced by the flow. Based on the angle of attack, the pitching moment about  $c/4$  was calculated from the corresponding values of the lift, drag, and pitching moment about  $c/2$ . The maximum error for these quantities is 5%.

## III. Results

Figure 5 shows lateral-view pictures of the model changing the shape of the upper surface with static actuation in still air. Figure 5a) is the model with actuation at the minimum voltage of -500 V whose shape is similar to the NACA 4415 airfoil. Figure 5b) shows the non-actuated model which has slightly flatter shape and Fig. 5c) shows the further flattening obtained by increasing the voltage to 1000 V. Although higher voltages could be applied to the

MFCs, these were not considered since they could introduce an excessive bending moment at the bond between the skin and the brass shim and furthermore they produced an unnaturally flat, or even concave, upper profile.

Figure 6 illustrates the displacement in the  $n$  direction of the upper skin measured at  $0.4 c$  from the leading edge of the model. Figure 6a) shows the actuation voltage and the corresponding skin displacement in still air during one actuation cycle between  $-500$  V and  $1000$  V. The voltage was kept constant for two seconds at the extremes of the voltage range as well as at the values of  $0$  V both increasing and decreasing the voltage. This corresponds to the time for acquiring the aerodynamic forces and moment of the model discussed below. A hysteresis loop is obtained by plotting the skin displacement as a function of the actuation voltage. This is an undesirable but typical behavior due to the piezo-ceramic bimorph nature of the MFC actuators.<sup>18</sup> Figure 6b) shows 5 such loops which almost perfectly overlap indicating excellent repeatability of the displacement with actuation. The arrows in the figure indicate the loop path. Points a, b, and c in Fig. 6b) match the corresponding shapes of Figs. 5. Point d is the alternative zero-voltage position, obtained increasing the voltage from the minimum to the maximum value, whose displacement is quite close to the one at  $-500$  V. The displacement of the skin at these constant voltage points exhibits a small amount of creep which is also visible in Fig. 6a). The non-actuated model at point b has an inward displacements of about  $1.4$  mm (corresponding to  $0.93\%$   $c$ ) compared to point a which is the reference position with actuation at  $-500$  V. Increasing the voltage to  $1000$  V, point c, produces a  $3.1$  mm inward displacement (corresponding to  $2.1\%$   $c$ ). Displacements corresponding to other points enclosed by the loop of Fig. 6b) can be obtained by varying the actuation voltage and depending on the previous deformation history of the MFCs.

Figures 6c) and 6d) show analogous data for the airfoil aerodynamically loaded at  $\alpha = 0^\circ$  in a  $U_\infty = 15$  m/s flow. A small positive displacement is observed with actuation at  $-500$  V which is attributed to the low pressure on the upper surface. In any case, the actuators are capable of contrasting the aerodynamic loads and to achieve deformations of the upper surface which are similar to those in still air. Similar results (not shown here) have been obtained at other angles of attack in the range between  $-6^\circ$  to  $14^\circ$ . The symbols in points a, b, and c of Fig. 6d) correspond to the aerodynamic states discussed next.

Wind-tunnel tests were performed at freestream velocities up to  $20$  m/s for values of the angle of attack ranging between  $-10^\circ$  to  $16^\circ$ . In this range of velocities and angles of attack, the upper skin of the model did not exhibit any vibration or anomalous deformation both without and with actuation from the minimum to the maximum voltages. As noted above, the response of the skin to actuation was comparable to that observed in still air.

Figure 7 compares the lift and drag coefficients of the model actuated at  $-500$  V to those of the NACA 4415 airfoil measured by Jacobs and Pinkerton.<sup>23</sup> The data, obtained at  $U_\infty = 15$  m/s for  $\alpha$  ranging between  $-6^\circ$  to  $14^\circ$ , are not corrected for the effects of tunnel blockage. Larger values of the angle of attack are not considered since these would be significantly affected by the blockage of the model (whose chord is comparable to the height of the wind-tunnel test section). At this velocity, the Reynolds number  $Re_c$  based on the chord of the model is about  $150,000$  and thus the flow around the model is laminar. Our data compare reasonably well with the NACA data even if the shape of our model is not exactly the same of the NACA 4415 airfoil and the flow regime of the NACA experiments is turbulent ( $Re_c > 3 \cdot 10^6$ ).

For the same conditions, Fig. 8 compares the aerodynamic characteristics of the airfoil model without and with actuation. The upper surface deforms inward and the airfoil becomes increasingly flatter when the voltage is increased from the minimum value. The lift coefficient correspondingly decreases by a small margin, Fig. 8a), except for  $\alpha$  between  $0^\circ$  and  $6^\circ$  for which this trend is reversed, a behavior warranting further analysis. The drag coefficient of the model also decreases especially for values of  $\alpha$  between  $0^\circ$  and  $6^\circ$ , the range of angles of attack typically used during cruise, Fig. 8b). However the flatter configuration (with actuation at  $1000$  V) has slightly higher drag coefficient than the other cases close to the extremes of the range of angles of attack tested. Figure 8c) shows the corresponding lift over drag ratio. It is clear that flattening the profile of the airfoil produces a more efficient configuration for cruise conditions by virtue of its lower drag compared to the other cases. Figure 8d) shows the corresponding lift-drag polars indicating that for  $C_L$  lower than 1 the inward displacement offers a performance advantage. Figures 8e) and 8f) show the pitching-moment coefficient about  $c/4$  and the non-dimensional chordwise position of the center of pressure as a function of the angle of attack, respectively. We can see from these figures that changing the shape of the airfoil does not adversely impact the pitching moment and that the location of the center of pressure, and thus the stability of the aircraft, is not affected at ordinary angles of flight ( $\alpha > 0^\circ$ ).

The data in Fig. 8 show that, in principle, the shaping of a surface by MFC actuators can be useful for tailoring the aerodynamic performance of an airfoil. In particular, this technique could be very beneficial to broaden and stabilize the useful aerodynamic envelope of high-performance airfoils that quickly deteriorate their characteristics at off-design conditions.

#### IV. Conclusion

An airfoil model has been designed and constructed that has a flexible upper skin whose shape can be changed by macro fiber composite (MFC) actuators bonded to its inner side. These piezoelectric actuators are very thin, light, robust, and have low power consumption. In the design discussed, they become an integral part of the upper skin of the model. The displacement of the skin with static actuation has been measured both in still air and in a 15 m/s wind-tunnel flow at different angles of attack. Static actuation at the minimum voltage of -500 V produces a shape similar to that of the NACA 4415 airfoil. Larger values of the voltage progressively flatten the upper profile of the airfoil with a maximum inward displacement of  $0.021 c$  achieved with actuation at 1000 V. The aerodynamically loaded skin did not show any vibration or anomalous deformation and maintained a response to the actuation comparable to that observed in still air. The undesirable but typical hysteresis of the MFC actuators can pose some difficulties in achieving a specified skin shape. Closed-loop control should be used in practical applications to overcome this problem and to actuate the skin to a desired aerodynamic shape. The aerodynamic characteristics of the airfoil have also been measured with a force balance. The results obtained indicate that larger values of the lift over drag ratio can be obtained by deforming the airfoil at angles of attack typical of cruise conditions without deteriorating the stability of an aircraft. These findings suggest that the shaping of a surface by MFC actuators can be useful for increasing the efficiency or for tailoring the aerodynamic performance of an airfoil. In particular, this technique could be very beneficial to broaden and stabilize the useful aerodynamic characteristics of high-performance airfoils that quickly deteriorate at off-design conditions.

## References

- <sup>1</sup> Reich, G. W., Bowman, J. C., and Sanders, B., "Large-Area Aerodynamic Control for High-Altitude Long- Endurance Sensor Platforms," *Journal of Aircraft* Vol. 42, No. 1, pp. 237.
- <sup>2</sup> Maute, K. K., and Reich, G. W., "Integrated Multidisciplinary Topology Optimization Approach to Adaptive Wing Design," *Journal of Aircraft* Vol. 43, No. 1, pp. 253.
- <sup>3</sup> Austin, F., Rossi, M. J., Van Nostrand, W., Knowles, G., and Jameson, A., "Static shape control for adaptive wings," *AIAA Journal* Vol. 32, No. 9, pp. 1895-1901.
- <sup>4</sup> Laxminarayana Saggere, and Sridhar Kota, "Static Shape Control of Smart Structures Using Compliant Mechanisms," *AIAA Journal* Vol. 37, No. 5, pp. 572.
- <sup>5</sup> Secanell, M., Suleman, A., and Gamboa, P., "Design of a Morphing Airfoil Using Aerodynamic Shape Optimization," *AIAA Journal* , Vol. 44, No. 7, pp. 1550-1562.
- <sup>6</sup> Siclari M. J., Van Nostrand, W., and Austin, F., "The design of transonic airfoil sections for an adaptive wing concept using a stochastic optimization method," AIAA Paper 96-0329.
- <sup>7</sup> Martins, A. L., and Catalano, F. M., "Drag optimization for transport aircraft Mission Adaptive Wing," *Journal of the Brazilian Society of Mechanical Sciences and Engineering* Vol. 25, No. 1, Jan./Mar. 2003.
- <sup>8</sup> Hubbard, J. E. Jr., "Dynamic Shape Control of a Morphing Airfoil Using Spatially Distributed Transducers," *Journal of Guidance, Control, and Dynamics*, Vol. 29, No. 3, pp. 612-616.
- <sup>9</sup> Munday, D., Jacob, J., and Huang, G., "Active Flow Control of Separation on a Wing with Oscillatory Camber," AIAA Paper 2002-0413, 40th AIAA Aerospace Sciences Meeting & Exhibit, Jan. 2002.
- <sup>10</sup> Munday, D., and Jacob, J., "Active Control of Separation on a Wing with Oscillating Camber," *Journal of Aircraft*, Vol. 39, No. 1, 2002, pp. 187-189.
- <sup>11</sup> Munday, D., Jacob, J., Hauser, T., and Huang, G., "Experimental and Numerical Investigation of Aerodynamic Flow Control Using Oscillating Adaptive Surfaces," AIAA Paper 2002-2837, 1st AIAA Flow Control Conference, June 2002.
- <sup>12</sup> Ehlers, S. M., and Weisshaar, T. A., "Static aeroelastic control of an adaptive lifting surface," *Journal of Aircraft* Vol. 30, No. 4, pp. 534-540.
- <sup>13</sup> Rocha, J., Moniz, P. A., Costa, A. P., and Suleman, A., "On Active Aeroelastic Control of an Adaptive Wing Using Piezoelectric Actuators," *Journal of Aircraft* Vol. 42, No. 1, pp. 278-281.
- <sup>14</sup> Weisshaar, T. A., and Duke, D. K., "Induced Drag Reduction Using Aeroelastic Tailoring with Adaptive Control Surfaces," *Journal of Aircraft* Vol. 43, No. 1, pp. 157-164.
- <sup>15</sup> Gern, F., Inman, D. J., and Kapania, R. K., "Computation of Actuation Power Requirements for Smart Wings with Morphing Airfoils," *AIAA Journal* Vol.43, No.12, pp. 2481-2486.
- <sup>16</sup> Pinkerton, J. L., and Moses, R. W., "A Feasibility Study To Control Airfoil Shape Using THUNDER," NASA Technical Memorandum 4767.
- <sup>17</sup> Bilgen, O., Kochersberger, K. B., Diggs, E. C., Kurdila, A. J., and Inman, D. J., "Morphing Wing Micro-Air-Vehicles via Macro-Fiber-Composite Actuators," AIAA Paper 2007-1785, *48th AIAA/ASME/ASCE/AHS/ASC Structures, Structural Dynamics, and Materials Conference*, Honolulu, Hawaii, Apr. 23-26, 2007.
- <sup>18</sup> Bilgen, O., Kochersberger, K. B., Inman, D. J., and Ohanian, O. J. III, "Novel, Bidirectional, Variable-Camber Airfoil via Macro-Fiber Composite Actuators," *Journal of Aircraft* Vol. 47, No. 1, pp. 303-314.
- <sup>19</sup> Bilgen, O., Butt, L. M., Day, S. R., Sossi, C. A., Weaver, J. P., Wolek, A., Mason, W. H., and Inman, D. J., "A Novel Unmanned Aircraft with Solid-State Control Surfaces: Analysis and Flight Demonstration," AIAA Paper 2011-2071, *52nd AIAA/ASME/ASCE/AHS/ASC Structures, Structural Dynamics, and Materials Conference*, Denver, Colorado, Apr. 4-7, 2011.
- <sup>20</sup> Bilgen, O., Saavedra Flores, E. I., and Friswell, M. I., "Implementation of a Continuous-Inextensible-Surface Piezocomposite Airfoil," AIAA Paper 2012-1902, *53rd AIAA/ASME/ASCE/AHS/ASC Structures, Structural Dynamics, and Materials Conference*, Honolulu, Hawaii, Apr. 23-26, 2012.
- <sup>21</sup> Moses, R. W., Pototzky, A. S., Henderson, D. A., Galea, S. C., Manokaran, D. S., Zimcik, D. G., et al., "Actively Controlling Buffet-Induced Excitations," report RTO-MP-AVT-123, Symposium on Flow Induced Unsteady Loads and the Impact on Military Applications, Apr. 2005.
- <sup>22</sup> Debiasi, M., Bouremel, Y., Khoo, H. H., Luo, S. C., and Tan, E. Z., "Shape Change of the Upper Surface of an Airfoil by Macro Fiber Composite Actuators", AIAA Paper 2011-3809, *29th AIAA Applied Aerodynamics Conference*, Honolulu, HI, June 2011.
- <sup>23</sup> Jacobs, E. N., and Pinkerton, R. M., "Tests of the N.A.C.A. Airfoils in the Variable Density Wind Tunnel. Series 44 and 64," National Advisory Committee for Aeronautics technical note No. 401, Dec. 1931.



Figure 1. Macro fiber composite (MFC) actuator [image courtesy of Smart Material Corp.].

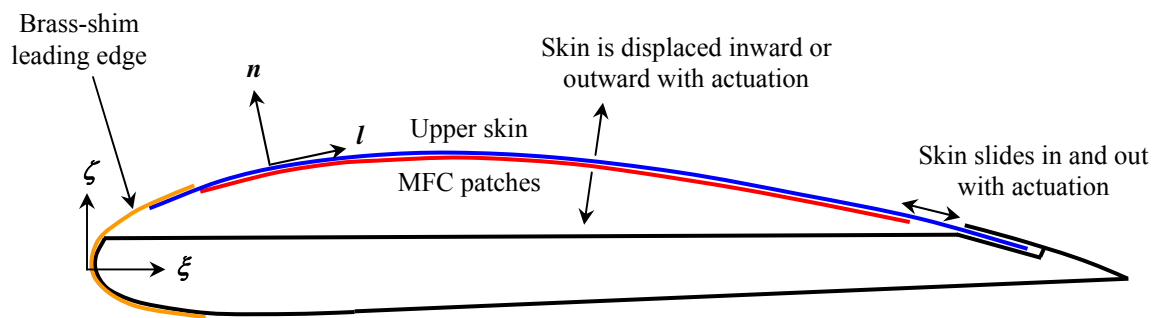
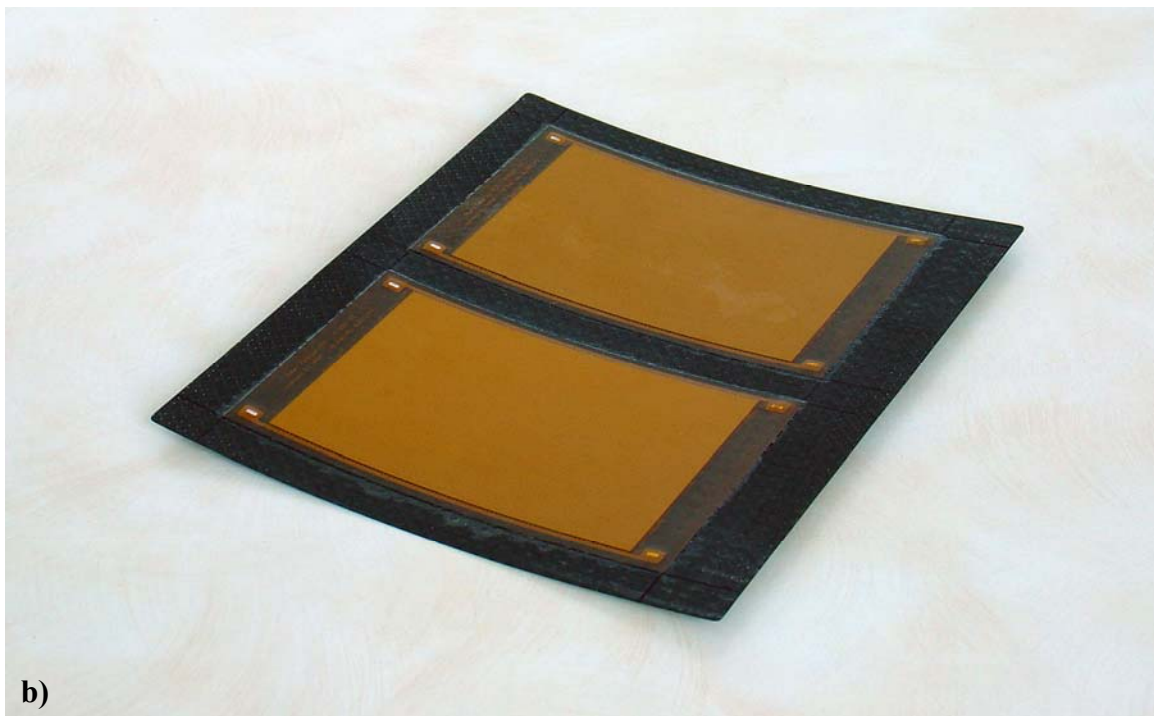
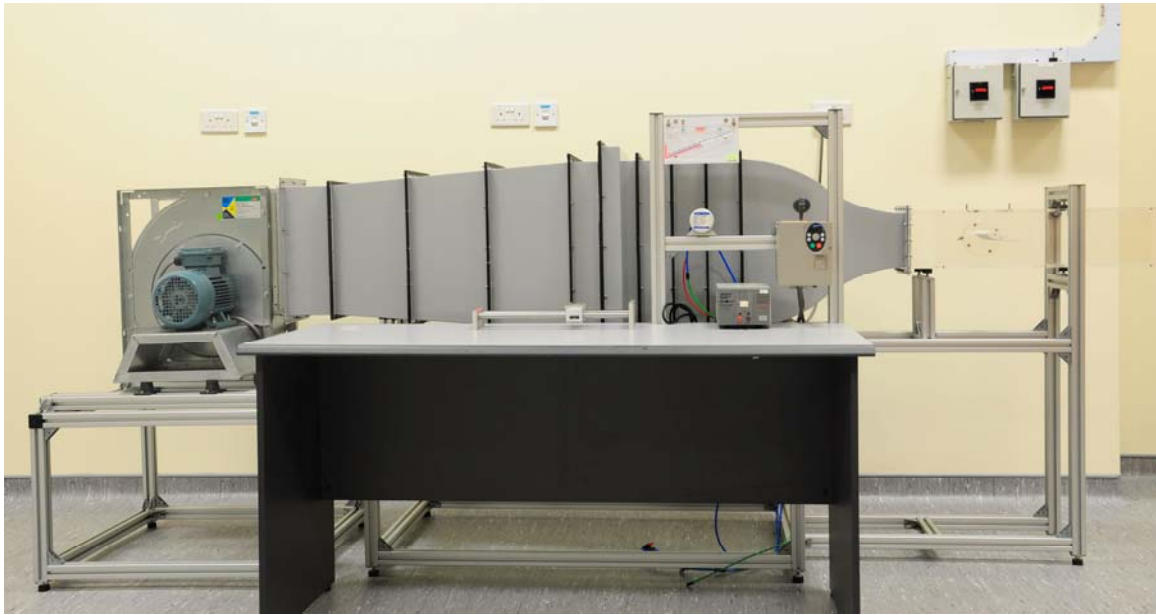


Figure 2. Schematic diagram of upper-surface actuation by MFC patches.



**Figure 3. Airfoil model for testing: a) assembled model; b) inner side of the carbon-fiber upper skin with MFC patches.**



**Figure 4. Small, open-loop, subsonic wind tunnel of the NUS Temasek Laboratories.**



**Figure 5. Lateral view of the airfoil model: a) with actuation at -500 V (shape similar to a NACA 4415 airfoil); b) without actuation (about 1.4 mm inward displacement); c) with actuation at 1000 V (about 3.1 mm maximum inward displacement).**

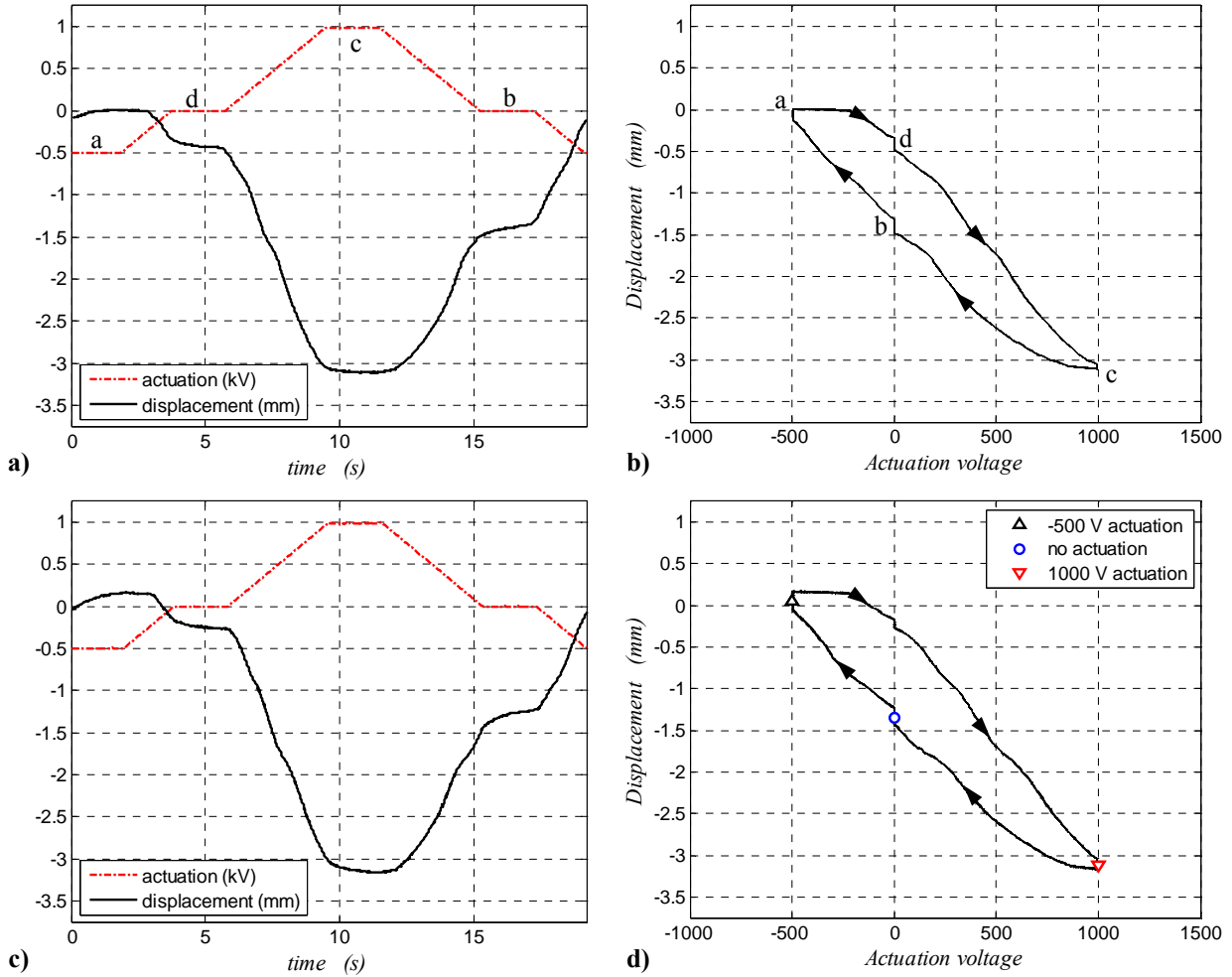


Figure 6. Displacement of the skin at 0.4 c: a) actuation and displacement, and b) hysteresis loop without flow; c) actuation and displacement, and d) hysteresis loop with aerodynamic load at  $\alpha = 0^\circ$  in a  $U_\infty = 15$  m/s flow.

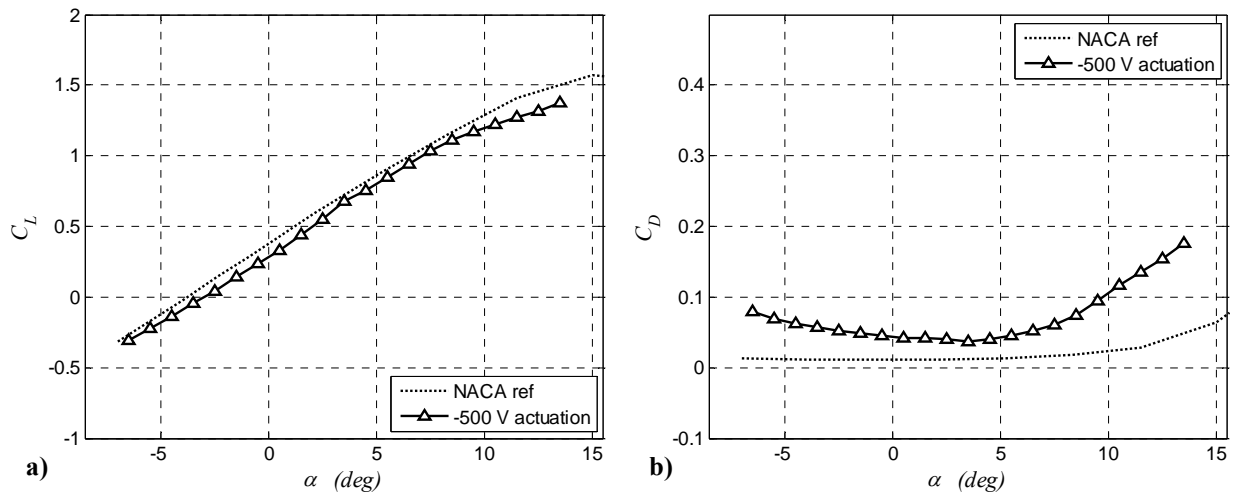


Figure 7. Comparison of NACA 4415 airfoil<sup>23</sup> and current model actuated at -500 V: a) lift coefficient; b) drag coefficient.

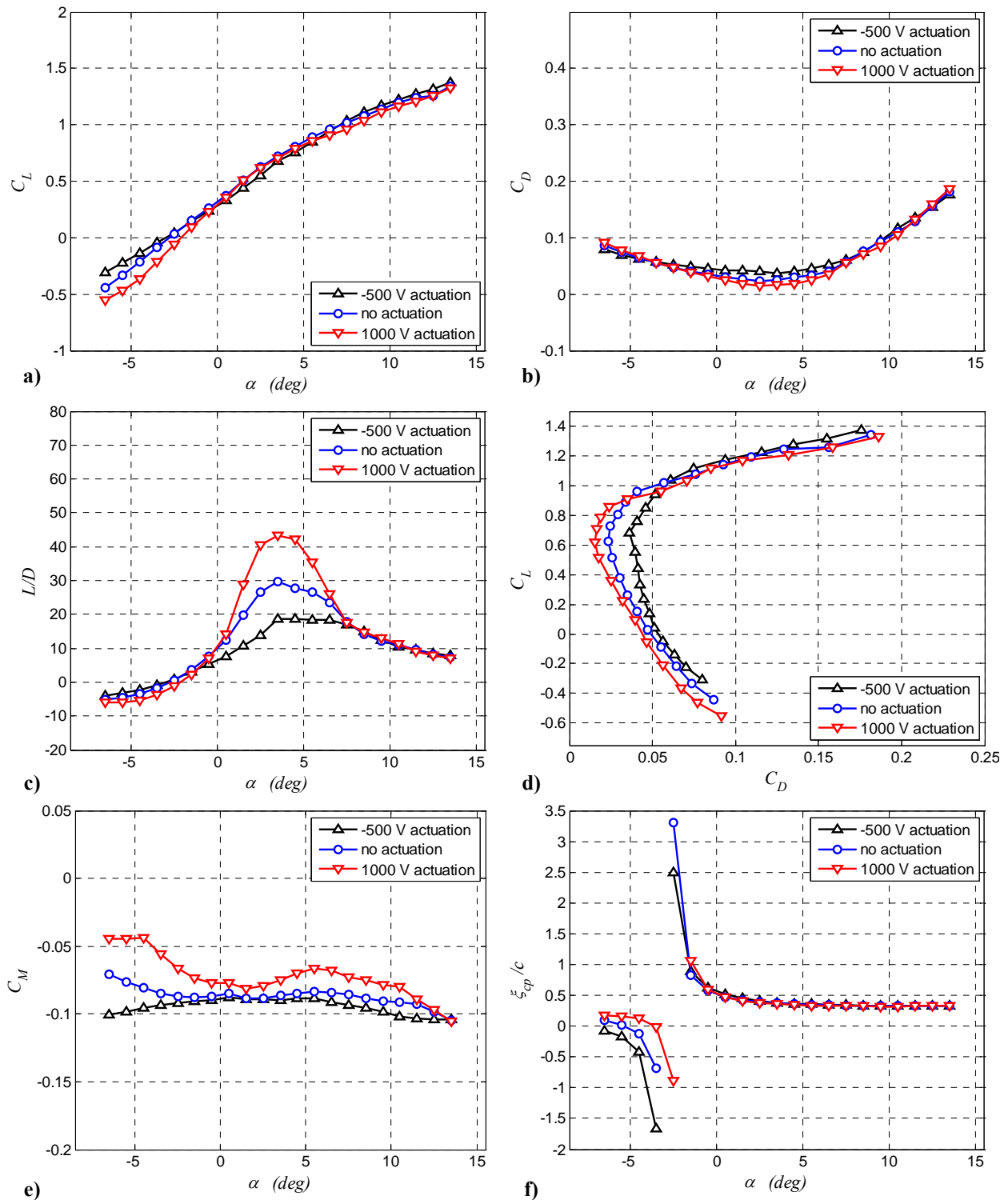


Figure 8. Aerodynamic characteristics of the airfoil model without and with actuation: a) lift coefficient; b) drag coefficient; c) lift over drag ratio; d) lift-drag polar; e) pitching-moment coefficient about  $c/4$ ; f) non-dimensional chordwise position of the center of pressure.